Journal of Applied Fluid Mechanics, Vol. 17, No. 11, pp. 2349-2360, 2024.
Available online at www.jafmonline.net, ISSN 1735-3572, EISSN 1735-3645.
https://doi.org/10.47176/jafm.17.11.2699

Heat Transfer and Entropy Generation in Vibrational Flow: Newtonian vs. Inelastic Non-Newtonian Fluid

S. K. Mishra†, A. Mishra, P. Singh and M. Dubey

Bhilai Institute of Technology, Durg, CG, 491001, India

†*Corresponding Author Email: santosh.mishra@bitdurg.ac.in*

ABSTRACT

A computational method is employed to solve heat transfer and entropy generation within a circular pipe. The thermal boundary condition assumes a constant wall temperature, while viscosity is taken to be dependent on temperature. A power-law type shear-thinning fluid is utilized in the analysis, with sinusoidal vibration applied horizontally perpendicular to the flow direction. Temperature distributions across the pipe are illustrated. Additionally, the entropy generation rate over the entire fluid volume under vibration was examined, comparing the results between steady flow and vibrational flow for both types of fluids. It was found that radial mixing is more pronounced in non-Newtonian fluids as vibration increases the strain rate, which is higher for low Reynolds numbers. The research provides a quantitative analysis of heat transfer and entropy generation for both Newtonian and shear-thinning fluids at different Reynolds numbers. It was observed that the effectiveness of superimposed vibrational flow is limited, especially for low Reynolds numbers and flow behavior index characteristic of shear-thinning fluids.

Article History

Received March 3, 2024
Revised April 23, 2024
Accepted May 8, 2024
Available online September 1, 2024

Keywords:

Laminar flow
Power-law fluid
Heat transfer coefficient
Bejan Number
Thermal entropy generation

1. INTRODUCTION

The non-Newtonian fluids, widely employed across various industries such as biomedical, pharmaceuticals, polymer melts, chemicals, and food processing, are sometimes utilized as a heat transfer fluid and at other times as the product to be processed itself. Thermal processes/heat transfer are broadly classified into two categories: active techniques, which involve external power to enhance heat transfer, and passive techniques, which include methods like the use of nanofluids, geometrical modifications, and inserts.

In the food processing sector, the continuous sterilization of high-viscosity liquid foods within laminar pipe flow is essential for preserving their nutritional attributes. To counter temperature fluctuations and ensure uniform radial distribution of temperature to maintain food quality, an active technique known as vibration is employed (Mishra, et al., 2019a; Gangadhar et al., 2022).

Vibration offers an alternative method for improving heat transfer by influencing the thermal dynamics of a system. With the potential to enhance convective heat transfer, it alters fluid flow behavior, leading to increased heat transfer efficiency. Vibration is employed in various industrial applications, including its use in spray cooling (Chen et al., 2023, 2024). It was found that the Nusselt number and cooling efficiency improve under conditions of low vibrational parameters and low Reynolds number flow. Specifically, at amplitude of 0.2 mm, the maximum heat transfer enhancement factor reaches 16% but subsequently diminishes with further increases in amplitude.

The pool boiling heat transfer process is notably influenced by mechanical vibration. According to Zhao et al. (2023), who conducted a review, pool boiling serves as a continuous heat source through latent heat during thermal processes, and vibration ensures the even distribution of bubbles, thereby promoting uniform heat transfer. This mechanism helps prevent bubble coalescence and enhances liquid replenishment on the heated surface, ultimately improving heat transfer efficiency.

Vibration can effectively be applied in heat exchangers to enhance the heat transfer and pressure drop i.e. pumping power. Setareh et al. (2019) documented a high heat transfer coefficient in their experimental study on a double pipe heat exchanger subjected to ultrasonic vibration. They investigated the impact of vibration at various temperatures and power levels.

Nomenclature

A	vibration amplitude, mm	T_f	bulk fluid temperature
Be	Bejan number	T_w	wall temperature
C_p	specific heat	$\bar{w}$	axial velocity (z-direction)
E_a	activation energy	***Greek symbols***	
f	vibration frequency	$\dot{\gamma}$	shear rate
h	heat transfer coefficient	μ	dynamic viscosity
k	fluid consistency index	μ_{eff}	effective viscosity
k_o	pre-exponential factor on Arrhenius model	λ	thermal conductivity
L	length of the pipe	ρ	fluid density
n	power-law index	***Subscripts***	
R	pipe radius	in	inlet
Re	Reynolds number	out	outlet
Re_v	vibrational Reynolds number	w	wall
Q	discharge	***Abbreviations***	
S	local total entropy generation rate	CFD	Computational Fluid Dynamics
$\dot{S}''_{TEG}$	local thermal entropy generation rate	TEG	Thermal Entropy Generation
$\dot{S}''_{FEG}$	local frictional entropy generation rate	FEG	Frictional Entropy Generation
S_T	total entropy generation	SF	steady state flow
ΔT_m	log-mean temperature difference	VF	Vibrated Flow

Mohammed et al. (2021) conducted experiments to examine the heat transfer performance of a concentric-type heat exchanger. Turbulators were placed inside the inner pipe and subjected to different types of vibrational signals to evaluate their performance. They concluded that high heat transfer was achieved regardless of the vibrational parameters when the turbulator was subjected to vibration.

Arasavelli et al. (2021) attempted to analyze the performance of a parallel flow concentric heat exchanger. They conducted a study by varying the frequency, acceleration, and position of vibration generation. In their experimental investigation, they concluded that maximum heat transfer enhancement (33%) was achieved for the combination of low frequency (40 Hz) and high acceleration (3 m/s^2).

A Computational Fluid Dynamics (CFD) investigation explored the flow characteristics in circular pipes using various types of fluids, with the application of vibrations aimed at enhancing heat transfer. Vibration notably improved temperature profiles, with enhancement ratios reaching 2.1 for Newtonian and 2.7 for non-Newtonian fluids. They have expanded their study to include nanofluids and determined that the use of nanofluids also resulted in enhanced heat transfer performance (Mishra, et al., 2019b; Mishra, et al., 2019c). Experimental work in vertical round tubes also showed increased critical heat flux enhancement with higher vibration intensity parameters.

In the pursuit of enhancing heat transfer within systems, a significant portion of the effort relies on the principles outlined in the first law of thermodynamics. While this approach yields valuable insights, it often falls short of identifying optimal conditions. Entropy Generation Analysis (EGA), rooted in the second law of thermodynamics, emerges as a powerful methodology for optimizing heat transfer processes. Pioneered by Bejan, entropy generation minimization represents a method for modeling and optimizing devices, effectively incorporating considerations of irreversibility inherent in thermal systems (Bejan, 1979).

Heat transfer and fluid friction represent the primary sources of irreversibility in fluid flow within a pipe. The temperature disparity between the fluid and the pipe wall leads to thermal irreversibility, while the viscosity of the fluid in motion induces frictional losses. Notably, viscosity emerges as the most influential property among various thermophysical properties, exerting significant effects on both heat transfer and pressure drop. Studies have extensively examined the impact of viscosity on entropy generation, particularly in smooth ducts experiencing laminar flows. The same analytical framework has been applied to analyze entropy generation in both laminar and turbulent flows within ducts subject to constant temperature, heat flux, and heat exchangers. Furthermore, investigations have delved into the entropy generation rate and the potential for thermodynamic improvement in helically coiled tubes under both cooling and heating conditions (Prattipati et al., 2021).

Zamzari et al. (2017) conducted numerical investigations into the impact of vibration on flow behavior, heat transfer, and entropy generation within an open cavity. They observed a significant increase in heat transfer and entropy generation rates as the vibration cycle's amplitude increased.

Esfahani and Shahabi (2010) investigated how non-uniform constant heat flux affected entropy generation in developing laminar pipe flow with a high Prandtl number fluid. They found entropy generation consistently exceeded cases with decreasing heat flux distribution, despite increasing distribution. The study solely focused on this condition, omitting alternatives like variable heat flux. Consequently, their optimization for minimizing entropy generation was limited to laminar flow, potentially restricting insights into real-world heat transfer systems.

Wang et al. (2018) conducted a numerical comparison of entropy generation in helically corrugated tubes and smooth tubes. They evaluated performance across various geometric parameters and Reynolds numbers, finding that thermal entropy generation gradients are higher near the wall of smooth tubes. Conversely, in helically corrugated tubes, vortices induced by secondary flow detach this region. The study doesn't explore severely turbulent pulsation regions, limiting its relevance.

Thermal transportation involves significant energy dissipation, which can be reduced by minimizing entropy formation within a thermal system. Entropy plays a crucial role across various domains, affecting process likelihood and efficiency. Processes like dissipation, mass transfer, chemical reactions, and heat transfer contribute to entropy generation. Minimizing entropy is key for enhancing the efficiency of equipment such as microchannels, chillers, reactors, and curved pipes.

The analysis above underscores the importance non-Newtonian fluids and vibration techniques in improving heat transfer efficiency across industries. Multiple studies illustrate how vibration effectively boosts heat transfer in applications such as food processing, spray cooling, and heat exchangers. While vibration enhances convective heat transfer in processes like spray cooling and heat exchangers etc., its effect on entropy generation remains unexplored. To optimize thermal processes, understanding the distribution of entropy generation is vital. Investigating entropy distribution aids in identifying regions of high irreversibilities, enhancing the design of efficient energy systems.

This study aims to explore entropy generation in a circular pipe, focusing on identifying concentration regions and enhancing energy efficiency. It investigates the flow of both shear-thinning and Newtonian fluids in a pipe, which is externally heated. It analyzes the heat transfer effect and thermal entropy generation in detail. Vibration is applied in the transverse direction, and the study explores how the Reynolds number and fluid type impact heat transfer and entropy generation. Moreover, the study investigates the variation of entropy generation rate throughout the fluid volume.

2. NUMERICAL SETUP

2.1 Governing Equations

In computational fluid dynamics (CFD), the finite volume method (ANSYS CFX, 2022) is employed to solve the following transport equations presented in cylindrical coordinates. The fluids are considered incompressible and irrotational in this context, with negligible viscous dissipation assumed.

Continuity equation

$$\frac{1}{r}\frac{\partial(ru_r)}{\partial r}+\frac{1}{r}\frac{\partial u_\theta}{\partial \theta}+\frac{\partial u_z}{\partial z}+\frac{\partial \rho}{\partial t}=0 \tag{1}$$

Radial Momentum equation

$$\rho\left(\frac{\partial u_r}{\partial t}+u_r\frac{\partial u_r}{\partial r}+\frac{u_\theta}{r}\frac{\partial u_r}{\partial \theta}+u_z\frac{\partial u_r}{\partial z}-\frac{{u_\theta}^2}{r}\right)=-\frac{\partial p}{\partial r}+\frac{1}{r}\frac{\partial(r\tau_{rr})}{\partial r}+\frac{1}{r}\frac{\partial \tau_{\theta r}}{\partial \theta}+\frac{\partial \tau_{zr}}{\partial z}-\frac{\tau_{\theta\theta}}{r} \tag{2}$$

***θ*-Momentum Equation**

$$\rho\left(\frac{\partial u_\theta}{\partial t}+u_r\frac{\partial u_\theta}{\partial r}+\frac{u_\theta}{r}\frac{\partial u_\theta}{\partial \theta}+u_z\frac{\partial u_\theta}{\partial z}+\frac{u_r u_\theta}{r}\right)=-\frac{1}{r}\frac{\partial p}{\partial \theta}+\frac{1}{r^2}\frac{\partial(r^2\tau_{r\theta})}{\partial r}+\frac{1}{r}\frac{\partial \tau_{\theta\theta}}{\partial \theta}+\frac{\partial \tau_{z\theta}}{\partial z} \tag{3}$$

Axial Momentum Equation

$$\rho\left(\frac{\partial u_z}{\partial t}+u_r\frac{\partial u_z}{\partial r}+\frac{u_z}{r}\frac{\partial u_z}{\partial \theta}+u_z\frac{\partial u_z}{\partial z}\right)=-\frac{\partial p}{\partial z}+\frac{1}{r}\frac{\partial(r\tau_{rz})}{\partial r}+\frac{1}{r}\frac{\partial \tau_{\theta z}}{\partial \theta}+\frac{\partial \tau_{zz}}{\partial z} \tag{4}$$

Here, u_r, u_θ and u_z are the velocity components in radial r, angular θ and axial z directions respectively.

Energy Equation

$$\rho C_p\left(\frac{\partial T}{\partial t}+u_r\frac{\partial T}{\partial r}+\frac{u_\theta}{r}\frac{\partial T}{\partial \theta}+u_z\frac{\partial T}{\partial z}\right)=\lambda\left[\frac{1}{r}\frac{\partial}{\partial r}\left(r\frac{\partial T}{\partial r}\right)+\frac{1}{r^2}\frac{\partial^2 T}{\partial \theta^2}+\frac{\partial^2 T}{\partial z^2}\right] \tag{5}$$

2.2 Entropy Generation

In CFX, user-defined functions are implemented to calculate the variation of entropy generation using the following equations (Wang et al., 2018)

$$\dot{S}_T''=\dot{S}_{TEG}''+\dot{S}_{FEG}'' \tag{6}$$

$$\dot{S}_{TEG}''=\frac{\lambda}{{T_f}^2}\left[\left(\frac{\partial T}{\partial r}\right)^2+\left(\frac{1}{r}\frac{\partial T}{\partial \theta}\right)^2+\left(\frac{\partial T}{\partial z}\right)^2\right] \tag{7}$$

$$\dot{S}_{FEG}''=\frac{\mu}{T_f}\left\{2\left[\left(\frac{1}{r}\frac{\partial r u_r}{\partial r}\right)^2+\left(\frac{1}{r}\frac{\partial u_\theta}{\partial \theta}\right)^2+\left(\frac{\partial u_z}{\partial z}\right)^2\right]+\left(\frac{1}{r}\frac{\partial u_r}{\partial \theta}+\frac{\partial u_\theta}{\partial r}\right)^2+\left(\frac{\partial u_r}{\partial z}+\frac{\partial u_z}{\partial r}\right)^2+\left(\frac{\partial u_\theta}{\partial z}+\frac{1}{r}\frac{\partial u_z}{\partial \theta}\right)^2\right\} \tag{8}$$

Where, λ is the thermal conductivity, μ is apparent viscosity and T_f is the bulk fluid temperature which is the mean temperature of inlet and outlet. Thus the total entry generation (S_T) and its component i.e. thermal entropy generation (S_{TEG}) and frictional entropy generation rate (S_{FEG}) are calculated through the volume integration over the computational domain as follows

$$S_T=\int \dot{S}_T''\,dV \tag{9}$$

The characterization of entropy generation relies on the Bejan number (Bejan, 1979). The local Bejan number (Be'') pertains to entropy generation at a specific point, while the average Bejan number (Be) accounts for the overall entropy generation within the system. The equations below are employed to compute these parameters.

$$Be''=\frac{\dot{S}_{TEG}''}{\dot{S}_T''} \tag{10}$$

$$Be=\frac{\int \dot{S}_{TEG}''dV}{\int \dot{S}_T''\,dV} \tag{11}$$

Bejan number ranges $0<Be<1$; if $Be>0.5$ thermal energy irreversibility dominates; else friction entropy dominates.

Table 1 Range of simulation parameters

Diameter, D $[mm]$	20
Length, L $[mm]$	500
Frequency, f $[Hz]$	50
Amplitude, A $[mm]$	2
Reynolds Number, Re $[-]$	$150-400$
Density, ρ $[kg\ m^{-3}]$	1000
Specific Heat capacity, C_p $[J\ kg^{-1}K^{-1}]$	4180
Thermal Conductivity, λ $[W\ m^{-1}K^{-1}]$	0.668

2.3 Numerical Procedures

The study considers both Newtonian and Non-Newtonian power-law type fluids. For Newtonian fluids, the apparent viscosity remains consistent at a given temperature. Conversely, in the case of non-Newtonian fluids, the apparent viscosity is contingent upon factors like pipe diameter and shear rate, etc. The following constitutive equations define the shear stress (Eq.12) and apparent viscosity (Eq.13) of power-law fluids.

$$\tau = k\dot{\gamma}^n \tag{12}$$

$$\eta = k\dot{\gamma}^{n-1} \tag{13}$$

Viscosity is greatly influenced by temperature and entropy generation so Arrhenius model is to calculate viscosity as follow Tian and Barigou (2015)

$$k = k_0\ exp\left(E_a/R_gT\right)^n \tag{14}$$

Where k_o is a pre-exponential factor

$[= 5e^{-7}$ & $5e^{-5}\ (Pa\ S^n)$ & $0.8]$, k is fluid consistency index, $E_a[= 35000\ kJmole^{-1}]$ is activation energy and R_g is the ideal gas constant. The simulation employs a range of parameters as illustrated in Table 1.

A 3D meshed pipe, 20 mm in diameter and 500 mm in length, is subjected to transverse vibration is x-direction, depicted in Fig. 1. Incompressible laminar flow is assumed regardless of the nature of the fluid, whether it is Newtonian or non-Newtonian. Equation 15 is used to calculate the velocity for different Reynolds number, cases examined (Chhabra & Richardson, 1999)

$$u_z = Re\ \mu_{eff}/\rho D \tag{15}$$

Where $\mu_{eff} = k((3n+1)/4n)^n(\ 8u_z/D)^{n-1}$is the effective viscosity of power-law fluid and it reduces to Newtonian fluid for $n = 1$. To ensure that the flow remains laminar in a transverse direction also for a given vibrational frequency and amplitude, an equation is used to calculate the vibrational Reynolds number (Mishra, et al., 2019d).

$$Re_v = \rho A 2\pi f D/\eta \tag{16}$$

2.4 Computational Grid and Boundary Conditions

A circular pipe's geometry is constructed in ANSYS ICEM CFD, with meshing as a pre-processing step. To ensure high accuracy, structural meshing was performed using hexahedral elements. Through the grid independence test, a grid of 4250 $cells/cm$ in the z-direction and 1150 cells in the $xy-$plane was established as optimal. To capture the variations near the wall, which exhibit high gradient values, inflation layers were generated with an increment factor of 1.2.

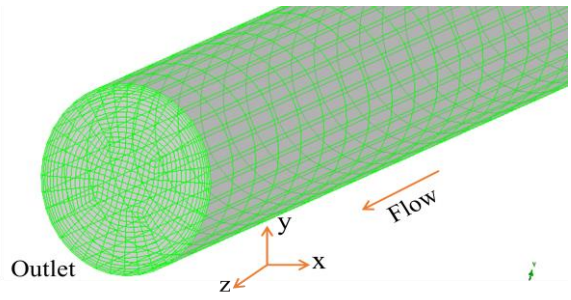

Fig. 1 Meshed geometry

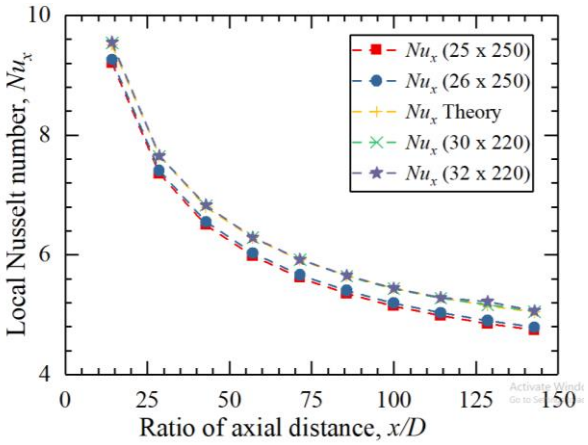

Fig. 2 Equation of thermally developing Hagen-poiseuille flow (Shah & Bhatti, 1987) used for Grid independency: $D = 7mm$; $L = 1\ m$; $q_w = 10500Wm^{-2}$; $T_{in} = 25$℃, $Re = 493.24$

Grid independence test was conducted to validate the variation of the local Nusselt number along the flow. It showed minimal deviation from the theoretical results for the grid size 30×220, as illustrated in Fig. 2. Additionally, no significant changes in results were observed upon further increasing the grid size. In Fig. 2, for instance, "$25x250$" denotes 25 divisions in the cross-sectional direction and 250 divisions in the axial direction.

Flow specifications were set up in CFX-Pre, and Table 2 summarizes the boundary conditions/initial conditions used. To expedite computational time, a fully developed velocity profile was ensured to capture heat transfer effects in a shorter pipe and demonstrate vibration effects. The problem was tackled in three steps: 1. Steady-state isothermal flow, 2. Steady-state thermal flow, and 3. Vibrational thermal flow. The inlet for the second and third simulations utilized a fully developed velocity profile. To address the advection term in the momentum equation, high-resolution advection schemes were employed. Additionally, to solve the transient term, 2nd order backward Euler schemes were selected to ensure both accuracy and boundedness.

Table 2 Summary of the applied boundary conditions/Initial Conditions

Surface	Boundary Conditions/ Initial conditions	
	Thermal	Momentum
Case 1: Isothermal Flow (SF)		
Intel	$T(r,\theta,0) = 20℃$	Velocity Inlet,
Outlet	-	Pressure outlet
Wall	$T(R,\theta,z) = 20℃$	No slip condition
Case 2: Steady State Thermal Flow (SF)		
Intel	$T(r,\theta,0) = 20℃$	Fully developed velocity profile from case 1
Outlet	-	Pressure outlet
Wall	$T(R,\theta,z) = 140℃$	No slip condition
Case 2: Non-isothermal Vibrational Flow (VF)		
Intel	$T(r,\theta,0) = 20℃$	Fully developed velocity profile from case 1
Outlet	-	Pressure outlet
Wall	$T(R,\theta,z) = 140℃$	No slip condition, Wall velocity, $v = A2\pi f\cos(2\pi ft)$ (Mishra, et al., 2020)

For vibrational flow simulations, the simulation time matches the flow residence time, which signifies the duration for the fluid to travel from inlet to outlet. To ensure accuracy, 12 iterations were established for each time step. Increasing the time step further extends the simulation time without a corresponding increase in accuracy. The time step is determined by dividing the time required to complete one cycle ($1/50\,Hz = 0.02\,s$) by 12, resulting in a time step of $0.00167\,s$. The root mean square error between two consecutive iterations for each time step has reached 10^{-6}, providing evidence of a satisfactory level of accuracy.

3. VALIDATION

Validating numerical simulations through comparison with experimental data, theoretical analyses, or previously published numerical simulation results is essential to ensure the accuracy and consistency of the simulation setup. Validation of the numerical simulation results for entropy generation was conducted by comparing them with the findings of Sahin and Ben-Mansour (2002). Their study investigated entropy generation in a circular pipe with a uniform wall heat flux boundary condition. They examined how the entropy generation rate varies across the fluid volume and compared the integrated entropy generation rate over the cross-sectional area with the simulated results, as detailed in Table 3.

In this context, as vibration is applied in the transverse direction, it becomes crucial to validate the simulation results specifically for transverse flow conditions. For this validation, the findings of Tian and Barigou (2015) were compared with the simulated

Table 3 Mean Entropy generation rate at several axial locations: $\rho = 998\ kg/m^3$, $C_p = 4182\ J/kg\ K$, $D = 25\ mm$, $L = 1\ m$, $q'' = 5000\ W/m^2$

Axial location (x/L)	Sahin and Ben-Mansour, 2002	CFD simulation	%Error
[-]	Mean entropy generation [W/mK]		
0	0.00365	0.00375	2.74
0.1	0.05532	0.0565	2.13
0.5	0.10130	0.1041	2.76
0.75	0.11527	0.11727	1.74
1.0	0.12520	0.12745	1.80

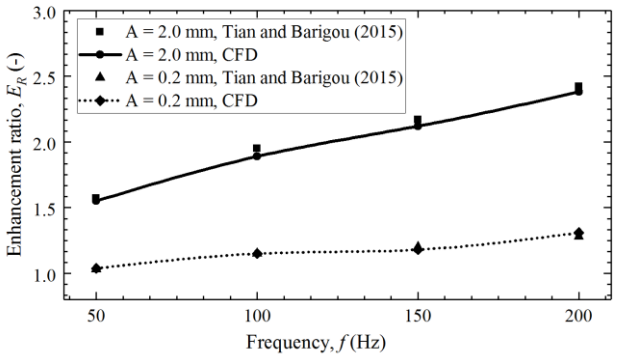

Fig. 3 Transverse vibration flow validation with Tian and Barigou (2015) results: $k = 1\ Pa\ s^n$, $n = 0.6$, $D = 4\ mm$, $L = 100\ mm$, $\Delta p/L = 20\ kPa\ m^{-1}$

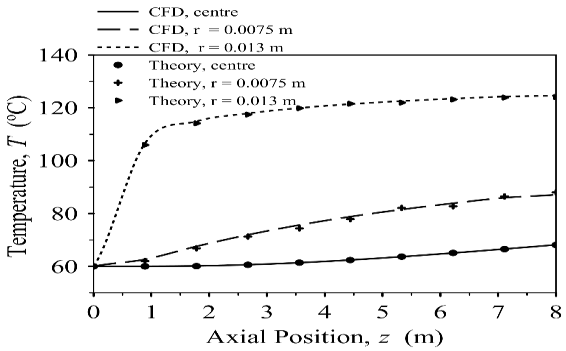

Fig. 4 Validation of axial temperature profile at various radial locations: $T_{in} = 60\ °C$; $T_w = 140\ °C$; $D = 30\ mm$; $\bar{w} = 0.04\ m\ s^{-1}$; $\mu = 0.001\ Pa\ s$; $\rho = 998\ kg\ m^{-3}$; $C_p = 4180\ J\ kg^{-1}K^{-1}$; $\lambda = 0.668\ W\ m^{-1}\ K^{-1}$

results, revealing a high level of accuracy with an error margin of approximately ±2%, as illustrated in Fig. 3.

Validation of temperature profile along the axial direction is essential for determining variations in entropy generation along the axis. To validate this, Tanner's (1985) work was referenced. Axial temperature variations were compared with CFD results at three different radial positions, as depicted in Fig. 4, demonstrating excellent agreement between CFD and theory (Tanner, 1985).

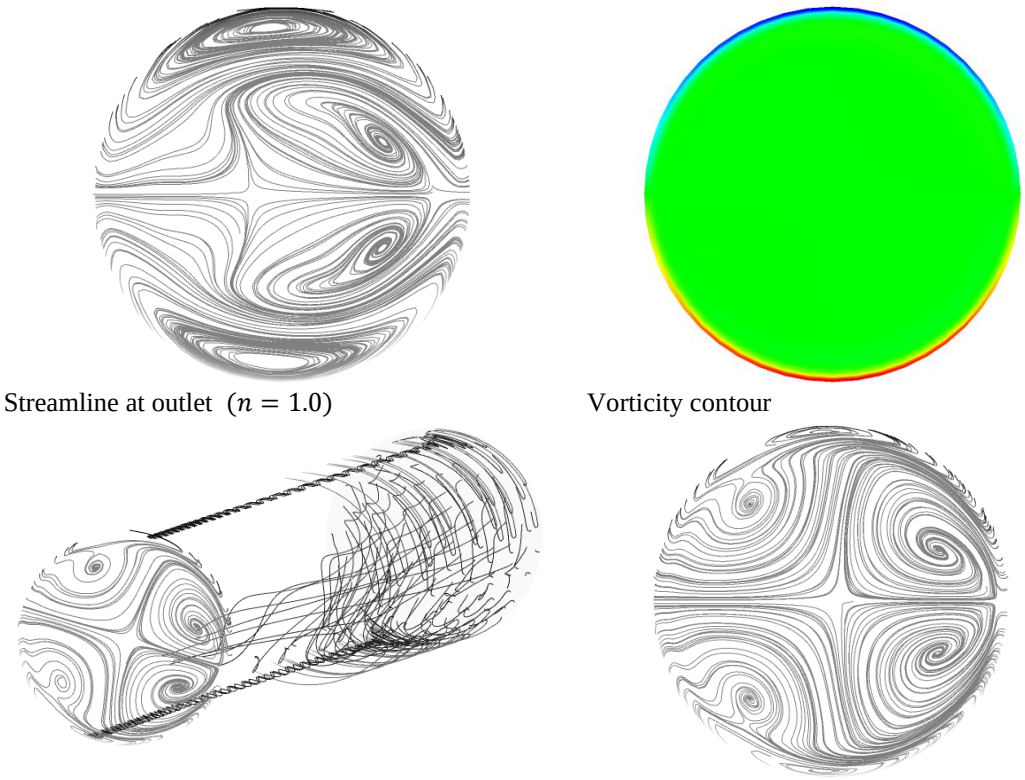

Streamline at outlet $(n = 1.0)$ Vorticity contour

Streamline along the length and at outlet $(n = 0.8)$

Fig. 5 Streamline and vorticity contour at various locations under vibrational flow $\mathbf{Re = 150, L = 500\ mm, D = 20\ mm}$

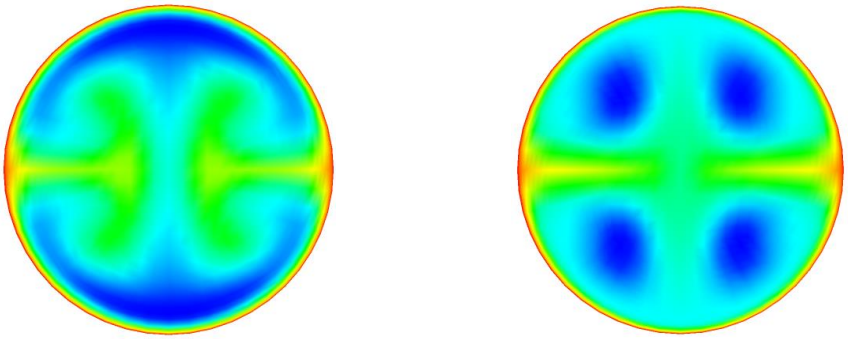

$n = 1.0$ $n = 0.8$

Fig. 6 Temperature distribution across the section at outlet under vibrational flow $\mathbf{Re = 150, L = 500\ mm, D = 20\ mm}$

4. RESULTS

The impact of vibration on heat transfer and entropy generation across varying Reynolds numbers for temperature-dependent viscosity has been numerically evaluated in both Newtonian and non-Newtonian fluids. Vibration proves to be an effective method for enhancing heat transfer by intensifying fluid layer agitation near the wall and promoting particle dispersion, thereby augmenting heat transfer rates. Figures 5-7 provide confirmation of this assertion. Vibration significantly enhances radial fluid mixing, influenced by frequency and amplitude, due to a swirling effect that fosters a more uniform temperature distribution along the tube.

In Fig. 5, streamline and vorticity contour maps are shown at the pipe exit subjected to vibrational flow. The illustration demonstrates the significant impact of radial mixing due to secondary flow produced by vibration. Similarly, Fig. 6 displays temperature contours for both Newtonian and non-Newtonian fluids. Temperature uniformity is higher in the case of non-Newtonian fluid compared to Newtonian fluid, attributed to the additional strain rate generated by vibration in the non-Newtonian fluid, whereas the Newtonian fluid remains unaffected by the strain rate. Figure 7 depicts temperature contours at various locations along the axial direction, illustrating the propagation of temperature variation under vibration conditions for demonstration purposes. Additionally, it presents the thermal entropy generation contour at the pipe outlet under vibration conditions.

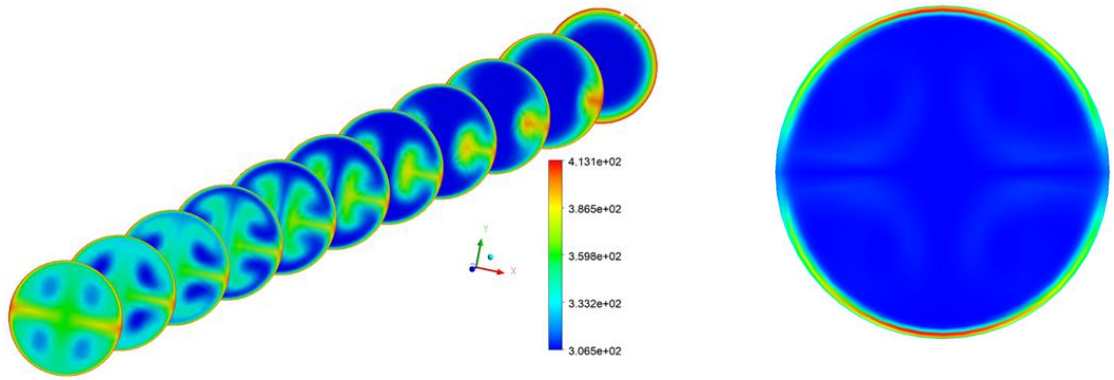

(a) (b)

Fig. 7 (a) Temperature distribution contour along the length under vibrational flow, (b) TEG contour at outlet $\mathbf{Re = 150, n = 0.8, L = 500\ mm, D = 20\ mm}, \boldsymbol{A = 2\ mm, f = 50\ Hz}$

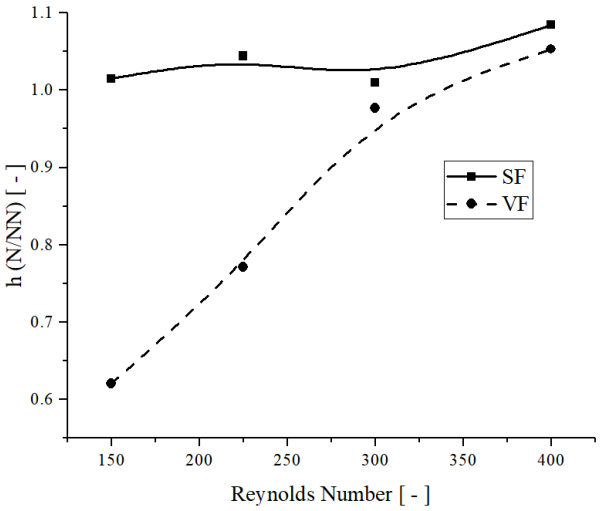

Fig. 8 Compression of ratio heat transfer coefficient of Newtonian to non-Newtonian fluid: $\boldsymbol{A = 2\ mm;;\ f = 50\ Hz, k =}$ Eq. (14)

The heat transfer coefficient values were determined using computational fluid dynamics (CFD) results in combination with the equation provided below.

$$\dot{m}C_p(T_{out} - T_{in}) = ha\Delta T_m \tag{17}$$

$$\Delta T_m = \frac{(T_w - T_{out}) - (T_w - T_{in})}{\ln[(T_w - T_{out})/(T_w - T_{in})]} \tag{18}$$

For steady-state flow (SF) of Newtonian fluids, the heat transfer coefficient increases with the Reynolds number, and similar trends are observed for non-Newtonian fluids. However, the values of the heat transfer coefficient for non-Newtonian fluids are lower compared to those for Newtonian fluids. At a Reynolds number of 400, the heat transfer coefficients are 595.1 and 548.7 ($W\ m^{-2}\ K^{-1}$) for Newtonian and non-Newtonian fluids, respectively. Conversely in vibrated flow (VF), the heat transfer coefficient decreases from its maximum to minimum value as the Reynolds number increases. In this case, for low Reynolds numbers, the heat transfer coefficient for non-Newtonian fluids is higher than that for Newtonian fluids. At a Reynolds number of 150, the heat transfer coefficients are 817.4 and 1316.3 for Newtonian and non-Newtonian fluids, respectively. Moreover, as the Reynolds number increases, the rate of decrement of the heat transfer coefficient for non-Newtonian fluids is greater than that for Newtonian fluids.

4.1 Newtonian Fluid Flow

In SF, close to the pipe inlet, temperature attains low values. Here, the fluid entering the pipe doesn't have adequate time to absorb heat from the pipe wall, resulting in a constant temperature pattern extending deeper into the fluid in this area and resulting in zero temperature gradient in this region. Hence TEG reduces, especially for low Reynolds numbers. With increasing pipe length, regions near the pipe wall develop higher temperature contours due to convective heating of the fluid in proximity to the pipe wall.

Figure 9 depicts the axial variation of the mean value of local thermal entropy generation (TEG) and Bejan number for various Reynolds numbers. At a Reynolds number of 400, the mean TEG is 80% greater than that of the flow at 150 Reynolds number. Additionally, the variation of the Bejan number is more pronounced for low Reynolds number flows, thus confirming the assertion that TEG exceeds viscous entropy generation for low Reynolds number flows. The constant increase in fluid temperature near the wall, attributed to the advection effect, contrasts with the stable temperature along the centerline, a consequence of the shorter pipe used in the simulation. Consequently, elevated TEG values are detected near the walls.

The centerline region experiences minimum TEG because bulk flows near these region exhibit nearly isothermal conditions, implying internal reversibility.

Figure 10 illustrates the axial changes in local thermal entropy generation (TEG) and the Bejan number for vibrational flow. It is observed that at a Reynolds number of 150, the maximum TEG occurs at 70% of the pipe length and subsequently decreases due to the enhanced mixing efficiency characteristic of low Reynolds number flows. Conversely, for higher Reynolds numbers, additional length is required to achieve significant fluid mixing. These trends are mirrored in the Bejan number,

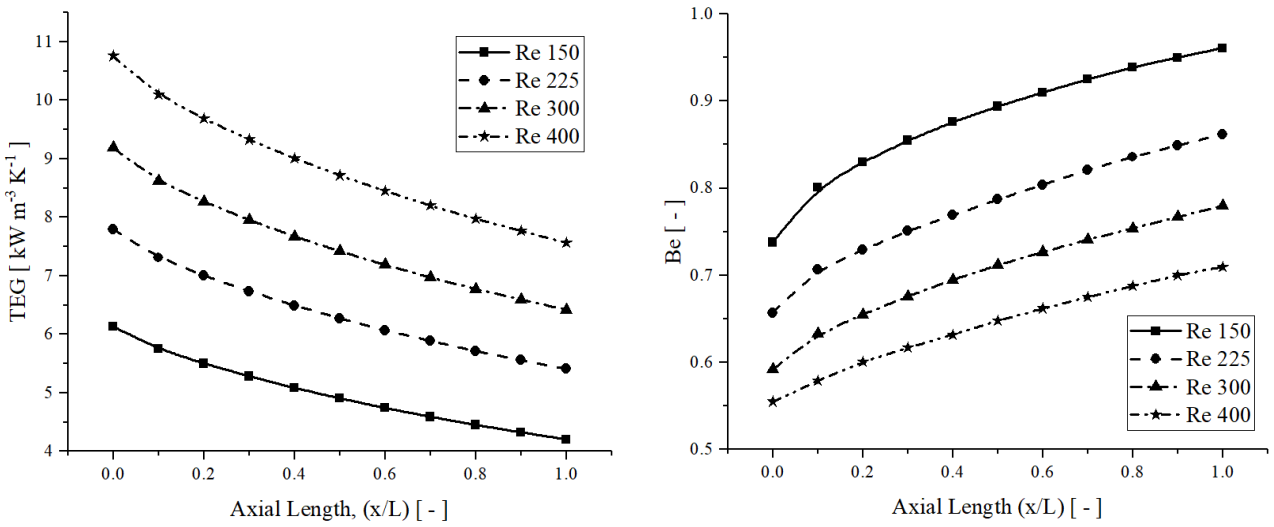

Fig. 9 Axial variation of local TEG and Be for steady flow of Newtonian fluid

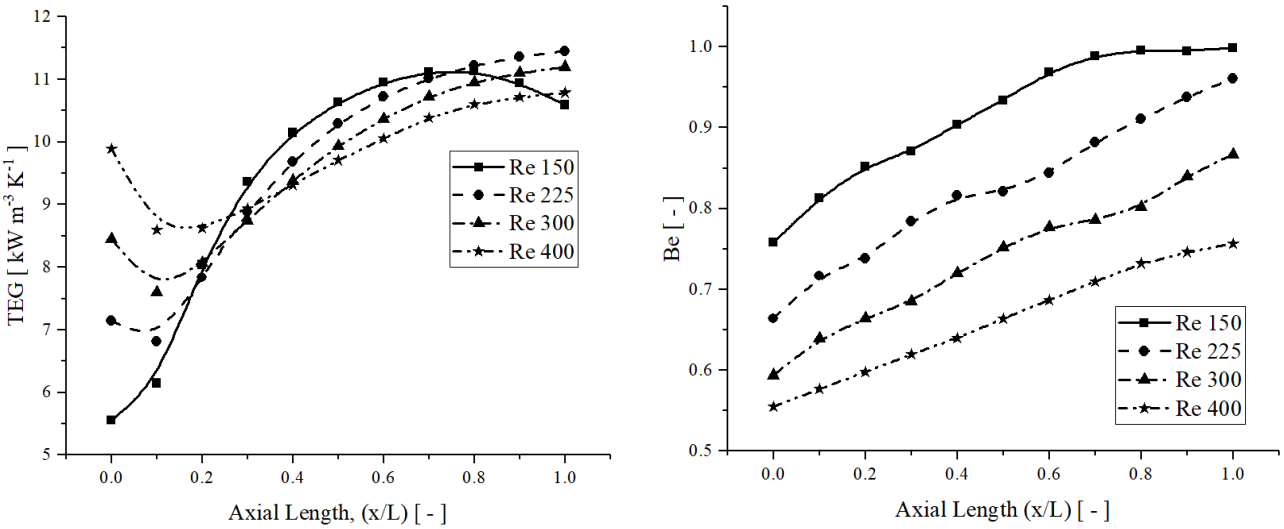

Fig. 10 Variation of local TEG and Be along the flow for vibrational flow of Newtonian fluid

where, for Reynolds number of 150, the mean temperature gradient remains relatively constant beyond 70% of the pipe length. By comparing TEG values between SF and VF, it becomes apparent that all cases of vibrational flow demonstrate elevated TEG in contrast to their respective steady flows. This variance can be attributed to the secondary flow components induced by vibration, which disrupt the thermal boundary layer and facilitate improved mixing. The Results imply that in SF, thermal entropy generation gradients are elevated near the wall, while in the case of VF, this region becomes detached due to vortices formed by secondary flow.

4.2 Non-Newtonian Fluid Flow

Figure 11 depicts the variations along the axis of local TEG and the Bejan number for SF conditions. At a Reynolds number of 400, the average TEG is 50% higher compared to the flow at a Reynolds number of 150. A similar trend is observed for the Bejan number as well, although the values are lower than those for Newtonian fluids. The reason for this phenomenon may be attributed to the fact that increasing the non-Newtonian parameter leads to a reduction in fluid friction near the pipe wall. Consequently, this results in lower entropy generation as the non-Newtonian parameter increases. In vibrational flow, entropy generation rises with the presence of a temperature gradient along the length. At low Reynolds number $Re = 150$, mixing occurs promptly, reaching its maximum value near the midpoint of the pipe, as illustrated in Fig. 12

Additional shear strain induced by vibration in non-Newtonian fluid enhances the mixing rate more effectively than in Newtonian fluid. This is why mixing is more prominent for low Reynolds numbers in non-Newtonian fluids compared to Newtonian fluids, leading to a more rapid decrease in the value of thermal entropy. Detailed comparison is discussed in the following section.

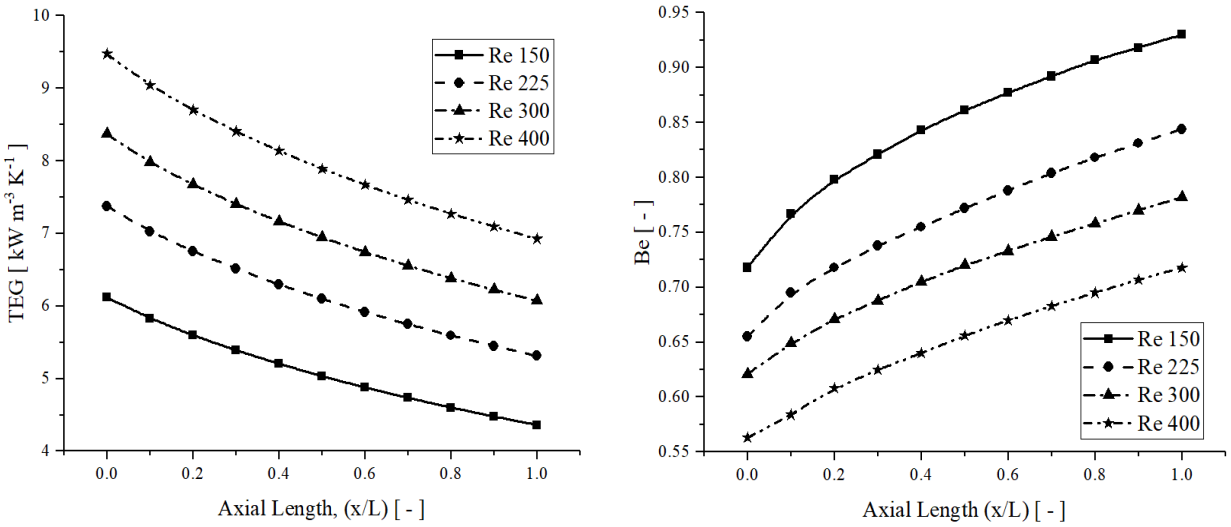

Fig. 11 Axial variation of local TEG and Be for steady flow of shear-thinning fluid

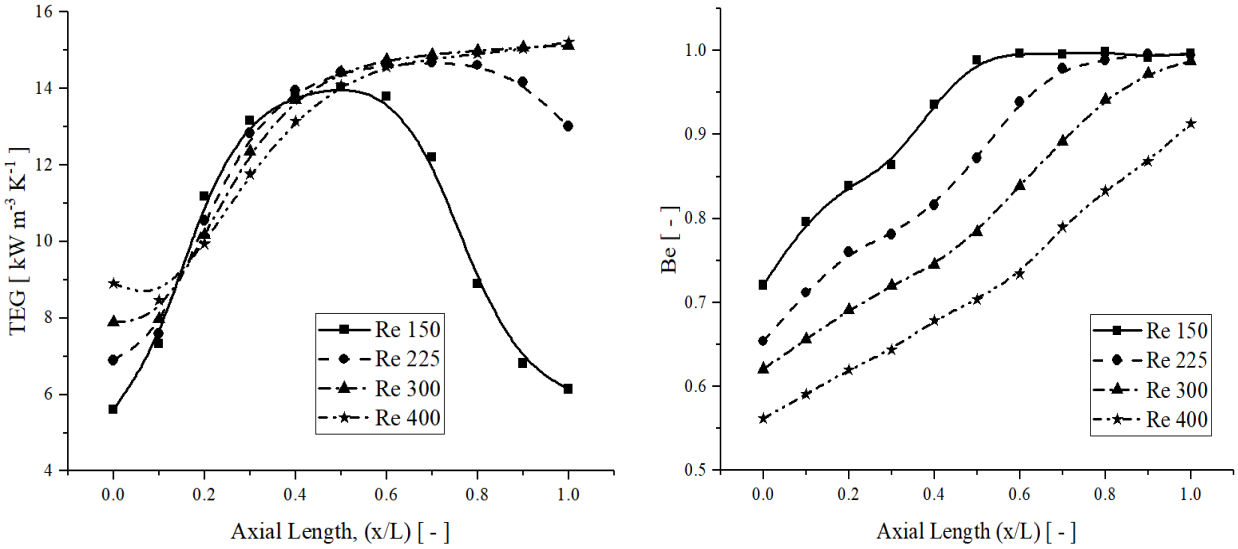

Fig. 12 Variation of local TEG and Be along the flow for the vibrational flow of shear-thinning fluid

4.3 Newtonian vs. Non-Newtonian Fluid Flow

In illustrating vibrational flow, Fig. 13 displays the variation of total entropy generation about the residence time of fluid within the pipe, denoting the duration required for fluid movement from inlet to outlet at various Reynolds numbers. Notably, the rate of increase in total entropy generation is significantly high for low Reynolds number flow irrespective of whether the fluid is Newtonian or Non-Newtonian. Specifically, at $Re = 150$, Newtonian fluid attends its maximum value at 50% of the residence and is almost constant for the remaining time whereas for non-Newtonian fluid it attends the value 40% of the time. Entropy generation remains relatively consistent across various relations for Newtonian fluid, as viscosity changes minimally with temperature. Conversely, significant differences in entropy generation are observed for non-Newtonian fluid due to variations in viscosity and strain rate effects.

Figure 14 (a) shows the total entropy generation of steady and vibrational flow. SF, illustrates that total entropy generation increases with the Reynolds number, and the rate of increment for Non-Newtonian fluid is 47% higher than Newtonian fluid at 400 Reynolds number. Conversely, in VF, the entropy generation for Newtonian fluid demonstrates minimal variation, while for non-Newtonian fluid, a considerable change is observed between Re 150 and 225, with subsequent increments showing near constancy.

Figure 14 (b) depicts the ratio of vibrational flow to steady state flow for both fluids across various Reynolds numbers. At $Re = 150$, VF/SF stands at 1.94 and 2.1 for n=1 and 0.8 respectively, while at $Re = 400$, VF/SF is 1.1 and 1.61 for $n = 1$ and 0.8 respectively. The figure highlights that the effect of vibration is more pronounced at low Reynolds numbers regardless of the fluid's nature. However, as the non-Newtonian parameter increases, the irreversibility value also increases. This phenomenon may be attributed to the additional strain rate induced by vibration, leading to enhanced fluid mixing.

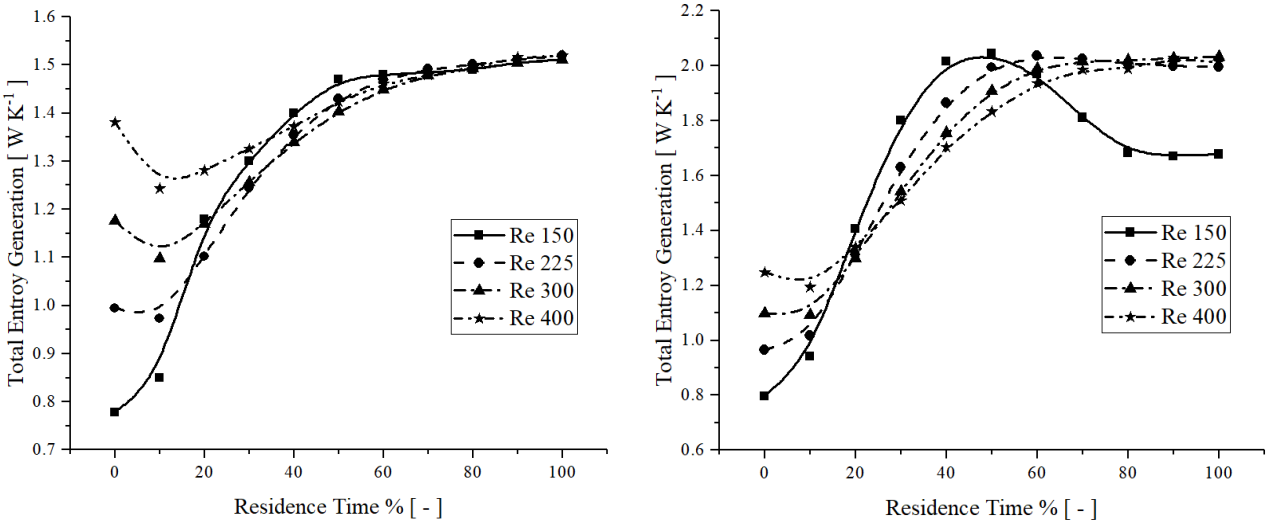

a) Newtonian fluid b) Non-Newtonian fluid

Fig. 13 Total entropy generation at outlet during residence time of vibrational flow

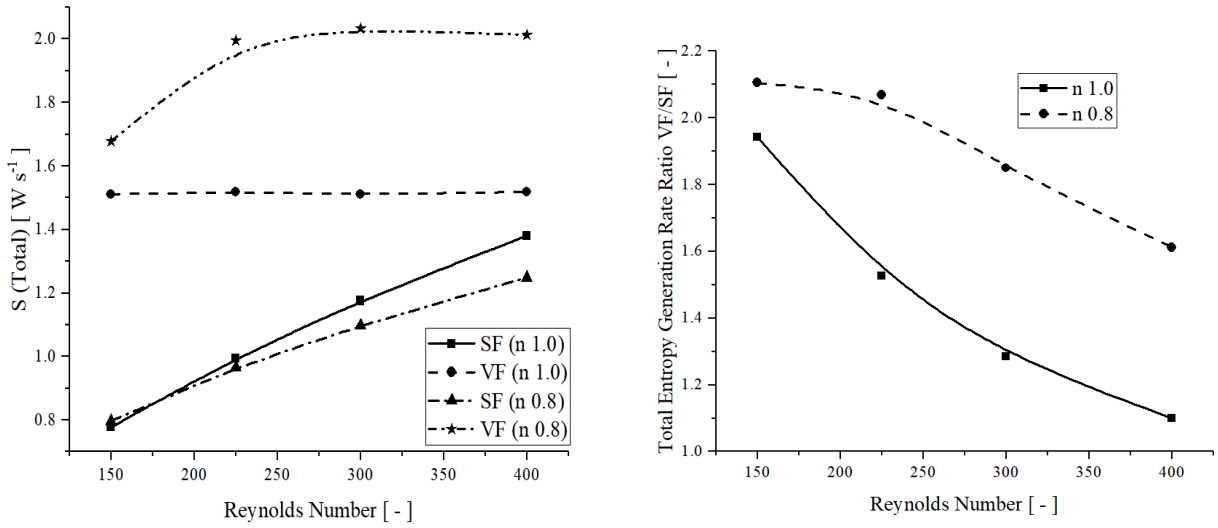

a) SF and VF b) VF/SF

Fig. 14 Total entropy generation rate of both fluids with Reynolds Number

Figure 15 depicts the variation of the ratio of total entropy generation between Newtonian and non-Newtonian fluids along the flow at various Reynolds numbers. In Fig. 15 (a), it can be observed that the value of TEG is higher for the Newtonian fluid throughout the length of the pipe in the case of steady-state flow, except for the scenario at the Reynolds number of 150. However, in vibrational flow, the initial ratio is decreasing across all Reynolds numbers, indicating that irreversibility is higher for the non-Newtonian fluid at the entrance of the pipe. As the flow continues, the non-Newtonian fluid achieves a higher level of mixing compared to the Newtonian fluid, resulting in a decrease in its irreversibility. This effect is more pronounced for low Reynolds numbers.

5. CONCLUSION

In conclusion, the investigation into heat transfer and entropy generation in Newtonian and non-Newtonian flows subjected to vibrational conditions within a pipe, with the accommodation of power-law fluids, yields several significant findings. Firstly, for steady-state flow, both types of fluids exhibit an increase in heat transfer coefficient with Reynolds number, with non-Newtonian fluids showing higher coefficients at low Reynolds numbers. Additionally, the Bejan number variation is more pronounced for low Reynolds numbers, emphasizing that thermal entropy generation surpasses viscous entropy generation in such conditions. A comparison between Steady Flow (SF) and Vibrational

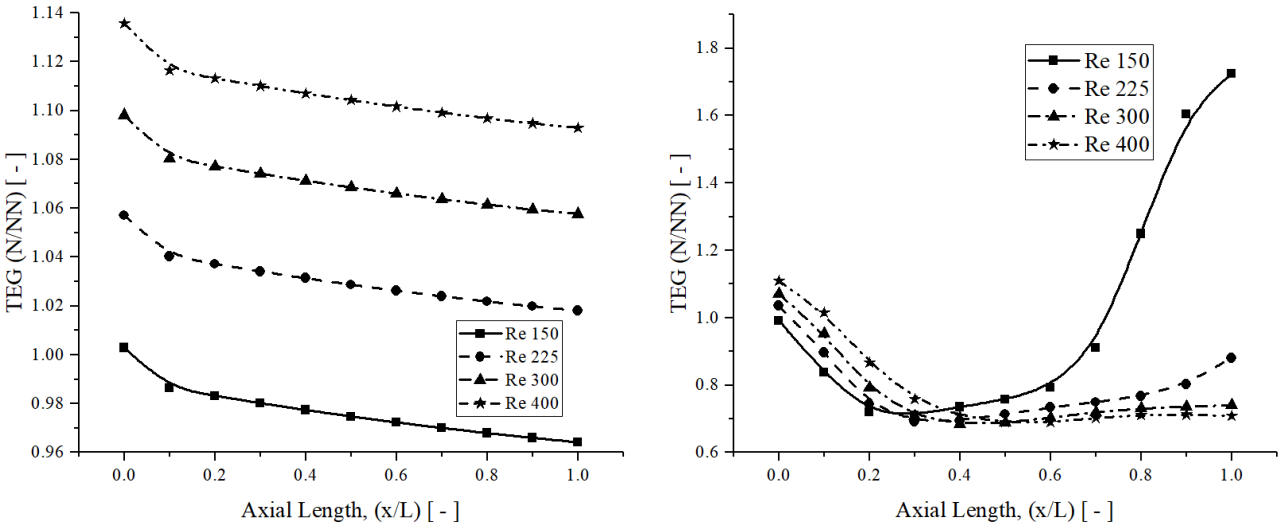

a) Steady Flow b) Vibrational flow

Fig. 15 Thermal Entropy Generation ratio of Newtonian to Non-Newtonian fluid along the flow

Flow (VF) indicates elevated thermal entropy generation in VF due to induced secondary flow components disrupting the thermal boundary layer and enhancing mixing. Notably, non-Newtonian fluids exhibit more pronounced mixing and a more rapid decrease in thermal entropy with vibration-induced shear strain. Moreover, the total entropy generation increases significantly at low Reynolds numbers, with distinct characteristics observed for Newtonian and non-Newtonian fluids. Transverse vibration induces strong vorticity fields and complex fluid motion, resulting in improved heat transfer and temperature profile development along the pipe. However, maintaining such conditions requires adjustments in vibration frequency and amplitude, particularly for low Reynolds numbers. Future research can extend these findings to more complex fluid mixtures and rheological behaviors to generalize the effects of vibrational flow on heat transfer.

CONFLICT OF INTEREST

No conflicts to disclose.

AUTHORS CONTRIBUTION

The authors confirm their contribution to the paper as follows: **Santosh Kumar Mishra**: Conceptualization, Data curation; **Mukesh Dubey**: Software; **Alka Mishra and Pushpendra Singh**: Validation. All authors reviewed the results and approved the final version of the manuscript.

REFERENCES

ANSYS CFX, U. M. (2022). ANSYS, Inc. USA.

Arasavelli, S., Konijeti, R., & Budda, G. (2021). Influence of transverse vibrations on convective heat transfer in parallel flow tube-in-tube heat exchanger. *Heat Transfer*, *50*(3), 1985-2006. https://doi.org/10.1002/htj.21965

Bejan, A. (1979). A study of entropy generation in fundamental convective heat transfer. *Journal of Heat Transfer*, *101*(4), 718-725. https://doi.org/10.1115/1.3451063

Chen, X., Du, A., Li, Z., Liang, K., Wang, X., Zhang, M., & Wang, Y. (2023). Heat transfer of single-phase spray cooling on heated vibrating surfaces. *Case Studies in Thermal Engineering*, *50*, 103489. https://doi.org/10.1016/j.csite.2023.103489

Chen, X., Du, A., Li, Z., Liang, K., Wang, X., Zhang, M., & Wang, Y. (2024). The effect of vibration on droplet dynamics and heat transfer of spray cooling. *Applied Thermal Engineering*, *238*, 122074. https://doi.org/10.1016/j.applthermaleng.2023.122074

Chhabra, R. P., & Richardson, J. F. (1999). *Non-Newtonian flow in the process industries: fundamentals and engineering applications.* Oxford: Butterworth Heinemann.

Esfahani, J., & Shahabi, P. (2010). Effect of non-uniform heating on entropy generation for the laminar developing pipe flow of a high Prandtl number fluid. *Energy Conversion and Management*, *51*, 2087-2097. https://doi.org/10.1016/j.enconman.2010.02.022

Gangadhar M, P., Rao, B. G., Sreenivasulu, B., & Arasavelli, S. S. (2022). Effect of vibration on heat transfer to laminar non-Newtonian nanofluid flowing through a circular pipe: A numerical analysis. *Numerical Heat Transfer, Part A: Applications*, *82*(11), 683-699. https://doi.org/10.1080/10407782.2022.2083862

Mishra, S., Chandra, H. S., & Arora, A. (2019a). Effects on heat transfer and radial temperature profile of non-isoviscous vibrational flow with varying Reynolds number. *Journal of Applied Fluid Mechanics*, *12*(1),

135-144. https://doi.org/10.29252/JAFM.75.253.28952

Mishra, S., Chandra, H., & Arora, A. (2019b). Application of vibration on heat transfer - A review. *I-manager's Journal on Future Engineering & Technology, 15*(1), 72-81. https://doi.org/10.26634/jfet.15.1.15877

Mishra, S., Chandra, H., & Arora, A. (2019c). Effect of velocity and rheology of nanofluid on heat transfer of laminar vibrational flow through a pipe under constant heat flux. *International Nano Letters, 9*, 245-256. https://doi.org/10.1007/s40089-019-0276-4

Mishra, S., Chandra, H., & Arora, A. (2019d). Numerical investigation of the effects of velocity and particle concentration on heat transfer of vibrational flow of non-newtonian nanofluid. *I-manager's Journal on Mathematics, 8*(1), 34-46. https://doi.org/10.26634/jmat.8.1.16239

Mishra, S., Chandra, H., & Arora, A. (2020). CFD study of heat transfer effect on nanofluid of Newtonian and non-Newtonian type under vibration. *Chemical Product and Process Modeling, 16*(4), 20200027. https://doi.org/10.1515/cppm-2020-0027

Mohammed, A., Kapan, S., Sen, M., & Celik, N. (2021). Effect of vibration on heat transfer and pressure drop in a heat exchanger with turbulator. *Case Studies in Thermal Engineering, 28*, 101680. https://doi.org/10.1016/j.csite.2021.101680

Prattipati, R., Narla, V. K., & Pendyala, S. (2021). Effect of viscosity on entropy generation for laminar flow in helical pipes. *Journal of Thermal Engineering, 7*(5), 1100-1109. https://doi.org/10.18186/thermal.977960

Sahin, A., & Ben-Mansour, R. (2002). Entropy generation in laminar fluid flow through a circular pipe. *Entropy, 5*(5), 404-416. https://doi.org/10.3390/e5050404

Setareh, M., Saffar-Avval, M., & Abdullah, A. (2019). Experimental and numerical study on heat transfer enhancement using ultrasonic vibration in a double-pipe heat exchanger. *Applied Thermal Engineering, 159*, 113867. https://doi.org/10.1016/j.applthermaleng.2019.113867

Shah, R. K., & Bhatti, M. S. (1987). Laminar convective heat transfer in ducts. In R. K. Shah, S. Kakac & W. Aung (Eds.), *Handbook of single phase convective heat transfer*. New York: Wiley.

Tanner, R. I. (1985). *Engineering Rheology*. Oxford: Clarendon Press.

Tian, S. and Barigou, M. (2015). *CFD modelling of oscillatory perturbed advection in viscous flows* [Ph.D. thesis, University of Birmingham]. Birmingham, UK.

Wang, W., Zhang, Y., Liu, J., Wu, Z., Li, B., & Sundén, B. (2018). Entropy generation analysis of fully-developed turbulent heat transfer flow in inward helically corrugated tubes. *Numerical Heat Transfer, Part A: Applications, 73*(11), 788-805. https://doi.org/10.1080/10407782.2018.1459137

Zamzari, F., Mehrez, Z., & Cafsi, A. (2017). Numerical investigation of entropy generation and heat transfer of pulsating flow in a horizontal channel with an open cavity. *Journal of Hydrodynamics, 29*, 632-646. https://doi.org/10.1016/S1001-6058(16)60776-X

Zhao, Y., Wu, H., & Dang, C. (2023). effect of mechanical vibration on heat and mass transfer performance of pool boiling process in porous media : a literature review. *Frontiers in Energy Research, 11*, 1288515. https://doi.org/10.3389/fenrg.2023.1288515